Effect of Substrate on the Diiron(III) Site in Stearoyl Acyl Carrier Protein Δ^9-Desaturase as Disclosed by Cryoreduction Electron Paramagnetic Resonance/Electron Nuclear Double Resonance Spectroscopy†

Roman Davydov,‡ Behnaz Behrouzian,§ Stojan Smoukov,‡ Joanne Stubbe,⊥ Brian M. Hoffman,*,‡ and John Shanklin§

Department of Chemistry, Northwestern University, 2145 Sheridan Road, Evanston, Illinois 60208-3113, Brookhaven National Laboratory, Department BO, Mail Stop 463, Upton, New York 11973-5000, and Department of Chemistry, Massachusetts Institute of Technology, Cambridge, Massachusetts 02139-4307

Received July 2, 2004; Revised Manuscript Received November 2, 2004

ABSTRACT: The diiron center in stearoyl-acyl carrier protein (ACP) desaturase (DS) from castor plant *Ricinus communis* catalyzes the dioxygen- and NADPH-dependent introduction of a cis double bond between C9 and C10 of stearoyl-ACP. Radiolytic reduction of diferric DS at 77 K produces an electron paramagnetic resonance (EPR)-detectable mixed-valence center (or $[DS_{ox}]_{mv}$) that is trapped in the conformation of the diferric precursor and thus provides a sensitive EPR/electron nuclear double resonance (ENDOR) probe of the structure of the diamagnetic diiron(III) state. The cryoreduced DS shows two distinct EPR signals, suggesting the presence of two diiron(III) states: the μ-oxo (major)- and μ-hydroxo (minor)-bridged diiron centers. ENDOR studies show that in the dominant oxo-bridged diferric state each iron(III) coordinates a histidine and a water along with other ligands. Samples containing stoichiometric amounts of stearoyl-ACP show pronounced changes in the EPR and ^{1}H ENDOR spectra of cryoreduced DS. EPR spectra of the cryoreduced DS−substrate complex reveal two distinct substates of the parent. EPR and ENDOR studies show that both major conformers of the diferric cluster have a μ-oxo bridge. ENDOR shows that the major conformer has a histidine and a water bound to both Fe ions. In the minor conformer, one of the irons has lost the terminal water ligand. The structure of the trapped $[DS_{ox}]_{mv}$ state relaxes upon annealing to 170 K: the μ-oxo bridge in the major cryoreduced DS species protonates on annealing to 170 K; this does not occur for the major DS−substrate complex, even upon annealing to 230 K. The relaxed Fe(II)Fe(III) center in cryoreduced DS and DS−substrate show much less intense and resolved ^{14}N ENDOR spectra than those of the structurally similar cryoreduced diiron center in ribonucleotide reductase (RNR) protein R2. This difference may reflect some differences in His−Fe bonds. The alterations in the diferric site of DS induced by substrate are suggested to be mediated by conformational changes in the polypeptide chain produced by substrate binding. These structural alterations may provide DS with an additional mechanism for tuning the redox potential of the diferric site. The mixed-valence states of DS are unstable at temperatures above 230 K.

The plant fatty acid desaturases catalyze the O_2- and NADPH-dependent insertion of a cis double bond in fatty acyl chains (*1*−*3*). For soluble forms of these enzymes, the substrate is covalently attached to acyl carrier protein (ACP)[1] via a phosphopantetheine thioester linkage (*4*). The best characterized ACP desaturase is the recombinant stearoyl-ACP Δ^9-desaturase (DS) from castor-oil plant *Ricinus communis* (*1*). This enzyme catalyzes the insertion of a cis double bond between carbons C9 and C10 of stearoyl-ACP (**1**-ACP) to generate oleoyl-ACP, which is a key intermediate in the biosynthesis of unsaturated cellular lipids. This enzyme is a homodimer of ∼42 kD subunits with each subunit having one binuclear iron site. Sequence alignment of the diiron cluster binding motif of the desaturase is similar to that in other class II diiron proteins such as R2 subunits of RNR and MMO (*5*−*7*).

Both the resting (diferric; DS_{ox}) and reduced (deferrous; DS_{red}) forms of DS have been studied. Optical and RR spectroscopy of the resting form provided compelling evidence for the presence of a μ-oxo bridge (*6*, *7*). According to RR spectroscopy, the Fe−O−Fe unit has an angle of ∼123° corresponding to a (μ-oxo)bis(μ-carboxylato)diiron-

† This work was supported by the NIH (Grant HL 13531, B.M.H.; Grant GM 2959, J. Stubbe) and the Office of Basic Energy Sciences of the U.S. Department of Energy (J. Shanklin and B.B.).

* To whom correspondence should be addressed. Phone: 847-491-3104. Fax: 847-491-7713. E-mail: bmh@northwestern.edu.

‡ Northwestern University.

§ Brookhaven National Laboratory.

⊥ Massachusetts Institute of Technology.

[1] Abbreviations: ACP, acyl carrier protein; Δ^9-desaturase, DS; DS_{ox}, diferric (resting) DS (as isolated); $[DS_{ox}]_{mv}$, DS_{ox} reduced at 77 K; **1**-ACP, stearoyl-ACP; **2**-ACP, 9-thiastearoyl-ACP; DS_{red}, diferrous DS; DS_{mv}, mixed-valence ACP; RNR R2 protein, subunit R2 of ribonucleotide reductase; EPR, electron paramagnetic resonance; ENDOR, electron nuclear double resonance; RR, resonance Raman; EXAFS, extended X-ray absorption fine structure; CD, circular dichroism; MCD, magnetic circular dichroism; CW, continuous wave.

10.1021/bi048599t CCC: $30.25
Published on Web 01/07/2005

(III) center, and the (μ-oxo) ligand is exchangeable with solvent (*6*, *7*). The presence of the Fe(III)−O−Fe(III) center in DS_{ox} was corroborated by high-field and variable-temperature Mossbauer measurements that showed antiferromagnetic coupling between high-spin iron(III) ions with $-J > 30$ cm^{-1} ($H = -2JS_1S_2$) (*6*). Mossbauer studies of the resting DS_{ox} revealed a disribution of spectroscopically distinguishable diiron(III) centers with $\Delta E_Q = 1.53$ (∼70%), 0.72 (∼21%), and 2.2 mm/s (∼7%) (*8*). The majority species contain diferric clusters of which the two iron sites are indistinguishable by Mossbauer spectroscopy. Further characterization of the DS_{ox} by EXAFS spectroscopy suggested the presence of distinct diiron clusters with Fe−Fe distances of either 3.12 or 3.41 Å, the former distance corresponding to the majority species (*8*). The center with the short Fe−Fe separation exhibits a 1.8 Å Fe−O bond and was proposed to represent a (μ-oxo)bis(μ-carboxylato)diiron(III) center, while the species with longer Fe−Fe separation contains no short Fe−O bonds and was suggested to represent a μ-hydroxo diiron(III) center.

Three-dimensional structures with resolution of 2.4 Å have been determined for DS_{red} (*9*) and recently for its azide and acetate complexes (*3*). The active-site structure shows two Fe(II) ions bound in a highly symmetric environment reminiscent of the dinuclear core in RNR R2: one iron is coordinated by Glu196 and His232, while the other iron is coordinated by Glu105 and His146 with both Glu196 and Glu105 binding in a bidentate mode. Two μ-1,3-carboxylate bridges, Glu229 and Glu143, span iron ions separated by 4.2 Å.

The diiron center is buried within polypeptide chains, and a prominent channel is proposed to be the substrate binding site. It starts at the surface of each subunit, bends at the diiron center, and then continues almost to the other end of the subunit (*2*). The bottom of this channel consists of mainly hydrophobic residues. Close to the surface at the narrow entrance of the substrate binding site, the channel is lined with Tyr292, Met265, Phe279, and Ser283. Overall, the substrate channel is boomerang shaped with a bend at the position of the iron cluster, placing the C9 carbon atom of stearoyl-ACP, where the double bond forms, at about 5.3 Å from the diiron center; a water molecule, which is in the second ligand sphere of the two iron ions, is between the diiron center and the C9 atom (*2*).

Recent CD and MCD studies showed that an addition of **1**-ACP to DS_{red} in molar ratio 1:1 significantly alters the geometric structure of both the Fe(II) ions, one becoming four-coordinate (*10*). The availability of an additional open coordination position on the four-coordinate center correlates with the observed enhancement of dioxygen reactivity in the presence of stearoyl-ACP (*11*). A recent RR study showed that stoichiometric addition of **1**-ACP to DS_{ox} caused small changes in the RR spectra of the Fe(III)−O−Fe(III) unit (*7*).

Diferric clusters in proteins and model compounds that are one-electron cryoreduced by γ-irradiation at 77 K produce an EPR-active mixed valence species, denoted $[DS_{ox}]_{mv}$ for the desaturase, that retains the conformation of the diamagnetic diferric precursor. EPR and ENDOR studies of such a state thus provide a sensitive structural probe of the EPR-silent diiron(III) center (*12*−*15*). In the present study, DS_{ox}, its substrate-bound form, and a substrate analog-bound form were cryoreduced and investigated with EPR and ENDOR spectroscopy. For comparison, analogous studies were carried out with RNR protein R2 the three-dimensional structure of which was determined and the diiron site of which is believed to be similar to that in DS (*5*−*7*). The mixed-valent species in such a nonequilibrium state relaxes to the corresponding equilibrium state upon annealing at higher temperatures (*12*−*15*), and we also report measurements on the relaxed desaturase, denoted DS_{mv}.

MATERIALS AND METHODS

Reagents and Proteins. All commercial reagents were used as obtained: HEPES buffer (Sigma), NaCl (Sigma), glycerol (Aldrich), D_2O (99.9 at. % D, Aldrich), glycerol-d_3 (Aldrich).

Recombinant *Escherichia coli* castor Δ^9-desaturase was expressed in *E. coli* strain BL21 gold (Novagen, Madison, WI) and purified as previously described (*16*). Stearoyl-ACP was prepared as previously described (*16*, *17*); 9-thiastearoyl-ACP was synthesized according to Behrouzian et al. (*18*). The protein−substrate complex was made by mixing either 0.5:1 or 1:1 of substrate/desaturase active site followed by concentration of the sample to 2.5 mM desaturase (active site). For samples in deuterated buffer, buffer exchange was effected by dialysis in two changes of deuterated buffer in a 10 kDa cutoff dialysis membrane (Spectrum Laboratories, Rancho Dominguez, CA) followed by concentration by ultrafiltration; substrates were then added, when appropriate. Protein samples were prepared in buffer, 0.02 M HEPES, pH 7, 60 mM NaCl, 16 vol % glycerol. The final concentration of DS was 2−2.5 mM (active site). *E. coli* RNR protein R2 was prepared as previously described (*19*).

The protein R2 samples were prepared in 0.1 M Tris/HCl, pH 7.4, buffer containing 16% glycerol. Protein R2 concentration was 2 mM (diiron site).

Methods. The procedures for radiolytic reduction of DS and RNR protein R2 at 77 K by γ-irradiation with ^{60}Co Gammacell 220 and for the subsequent annealing at different temperatures have been described elsewhere (*12*−*15*, *20*). Analysis of desatarase activity before and after irradiation showed no significant changes in specific activity, indicating that the treatment is not destructive. Likewise, the spectrometer for collecting 35 GHz EPR and ENDOR at 2 K has been described (*21*). X-band EPR spectra at 77 K were recorded on a modified Varian E 104 spectrometer.

The first-order ENDOR spectrum of nucleus with $I = {}^1/_2$ in a single paramagnetic center consists of a doublet centered at the Larmor frequency features with frequencies given by Abragam and Bleaney (*22*), $\nu_\pm = |\nu_N \pm A/2|$, where ν_N is the nuclear Larmor frequency and A is the orientation-dependent hyperfine coupling constant. For ^{14}N ($I = 1$), a single orientation gives a four-line pattern

$$\nu_\pm = |\nu_N \pm A/2 \pm 3P/2| \quad (1)$$

in which both the ν_+ and ν_- branches described by eq 1 are further split into two lines by the quadrupole splitting, $3P$. A full hyperfine tensor is determined from analysis of a 2D field-frequency plot comprised of spectra collected across the EPR envelope (*23*).

RESULTS

EPR of Cryoreduced Resting DS—Effect of Substrate. Figure 1 presents the 2 K Q-band EPR spectrum of $[DS_{ox}]_{mv}$

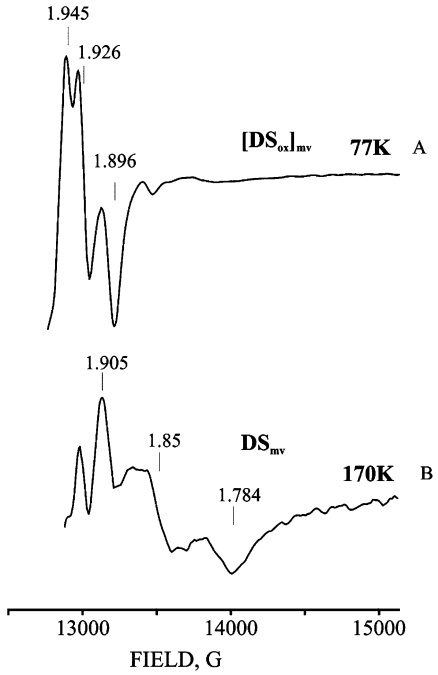

FIGURE 1: EPR spectra of resting desaturase radiolytically reduced at 77 K (A) and after its annealing at 170 K (B) for 1 min. Instrument conditions were as follows: $T = 2$ K; MW frequency = 35 GHz; 100 kHz modulation amplitude = 1.5 G; MW power = 30 dB.

Table 1: **g** Tensors for Cryoreduced Desaturase and RNR Protein R2

protein	$T_{annealing}$ (K)	species	g_1	g_2	g_3
R2	77	**a**	1.936	1.936	1.821
DS	77	**S1**[a]	1.945	1.926	1.898
	170	**S2**[b]	1.905	1.850	1.784
DS−**1**-ACP	77	**S3**[a]	1.938	1.938	1.727
	77	**S4**[c]	∼1.945	1.840	1.765
	174	**S4**[c]	∼1.945	1.840	1.765
DS−**2**-ACP	77	**S5**[a]	1.937	1.937	1.754
		S6[c]	∼1.94	1.860	1.797
		S7[c]	∼1.94	1.836	1.757

[a] Observable at 77 K. [b] Only observed below ∼30 K. [c] Observable at 77 K, but broadened.

prepared by radiolytic reduction of DS_{ox} at 77 K. $[DS_{ox}]_{mv}$ shows a rhombic EPR signal, **S1**, with g values of 1.945, 1.926, and 1.898 (Table 1) that also is detectable at 77 K (Figure S1). The structurally similar diiron(III) center of radical-free RNR protein R2 shows a comparable EPR signal with **g** tensor [1.936, 1.936, and 1.821] (Table 1). As shown previously (*12*−*15*, *24*, *25*), such a **g** tensor, as well as the slow spin relaxation, permits EPR detection at 77 K and is characteristic of the strong antiferromagnetic coupling provided by a μ-oxo bridge in a mixed-valent diiron(II,III) cluster. In contrast, μ-hydroxo-bridged diiron(II,III) clusters have relatively weak antiferromagnetic coupling and give more anisotropic EPR signals detectable only at helium temperatures (*13*−*15*, *24*, *26*). The EPR properties of the $[DS_{ox}]_{mv}$ **S1** species thus indicate the presence of the μ-oxo bridge in this majority fraction of the parent DS_{ox}. In Figure 1, one can also see weak higher-field resonances with greater **g**-anisotropy; these likely are due to cryoreduction minority substates of DS_{ox} that have hydroxo-bridged diferric sites. The low intensity prevents characterization of this signal(s).

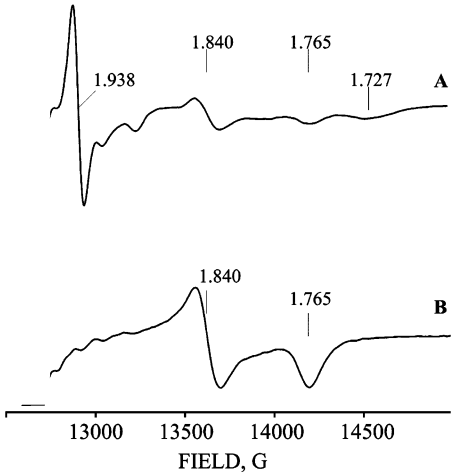

FIGURE 2: EPR spectra of cryoreduced 1 mM desaturase in the presence of 2 mM **1**-ACP: (A) irradiated at 77 K; (B) annealed at 175 K for 1 min. Instrument conditions were the same as those in Figure 1.

The addition of ACP (lacking the stearoyl group attached to the phosphopanteiene sulfhydryl) caused no changes in the EPR properties of the corresponding $[DS_{ox}]_{mv}$ (not shown). Cryoreduction of DS_{ox} in the presence of 0.5 and 1 M equivalents of **1**-ACP per iron center generated EPR spectra that contain new signals the intensity of which increases with the substrate/diiron site molar ratio. With the **1**-ACP/diiron site ratio of 1:1, ∼85% of the intensity is associated with these $[DS_{ox}-\mathbf{1}\text{-ACP}]_{mv}$ species. $[DS_{ox}-\mathbf{1}\text{-ACP}]_{mv}$ (1:1) exhibits two distinct EPR signals: one axial (**S3**), $g_\perp = 1.938$, $g_\parallel = 1.727$, and one rhombic (**S4**), **g** = [∼1.945, 1.84, and 1.765] (Figure 2, Table 1), which, respectively, account for ∼60% and 25% of the total cryoreduced DS in the presence of **1**-ACP 1:1. In spectra taken at 77 K, the axial signal is seen without any broadening (Figure S2, Supporting Information), whereas the rhombic signal **S4** broadens at 77 K.

These observations imply that (a) **1**-ACP forms a tight complex with DS_{ox} at molar substrate/iron site ratio of 1:1, (b) substrate binding induces conformational changes in DS_{ox}, which are reflected in the EPR properties of the mixed-valent $[DS_{ox}]_{mv}$ form generated at 77 K, and (c) the two spectroscopically distinct $[DS_{ox}-\mathbf{1}\text{-ACP}]_{mv}$ signals imply the presence of two different conformers of the substrate complex of the oxidized enzyme. The EPR properties of the species **S3** suggest that it contains a μ-oxo-bridged diferric center. The rhombic signal **S4** is noticeably broadened at 77 K**,** consistent with a diferric conformation having either a μ-oxo or μ-hydroxo bridge; as shown below, ^{1}H ENDOR data are consistent with the presence of μ-oxo bridge in the diiron-(III,II) center of this conformer and thus in the DS_{ox} parent.

Titration of DS_{ox} with 9-thiastearoyl-ACP (**2**-ACP), a structural analogue of the substrate, also shows the formation of a 1:1 complex. Its EPR spectrum is a superposition of four distinct EPR signals (Table 1) (*18*): a major axial signal **S5** with **g**-tensor [1.937, 1937, 1.754] and three less-intense rhombic signals **S1**, **S6**, and **S7** (Table 1, Figure S3A, Supporting Information).

The signal **S1** results from cryoreduced resting DS ($[DS_{ox}]_{mv}$). The signals **S5** and **S7** are similar but not identical to these **S3** and **S4** for $[DS_{ox}-\mathbf{1}\text{-ACP}]_{mv}$ (Table 1). The population of **S5** in cryoreduced $[DS_{ox}-\mathbf{2}\text{-ACP}]_{mv}$ is less than

the corresponding **S3** species in $[DS_{ox}-$**1**-ACP$]_{mv}$. The EPR data thus demonstrate that even the relatively small structural changes in the substrate associated with replacement of C9 for sulfur influence the substrate affinity for DS and the structure of the bound complex.

The $[DS_{ox}]_{mv}$ state and the $[DS_{ox}-$substrate$]_{mv}$ complexes with **1**-ACP and **2**-ACP relax to the equilibrium mixed-valence state at temperatures above 77 K. In the case of $[DS_{ox}]_{mv}$, the primary mixed-valence signal disappears and there appears a new, more anisotropic EPR signal **S2** with **g** = [1.905, 1.85, 1.79], detectable only at helium temperatures (Figure 1; Table 1). Such an EPR signal is likely due to an Fe(II)Fe(III) cluster with a μ-OH^- bridge (*15*−*18*, *20*−*22*, *24*). This signal gets slightly more heterogeneous after annealing at 230 K, and the sample shows no EPR signal after annealing at 240 K.

Annealing of $[DS_{ox}-$**1**-ACP$]_{mv}$ to 175 K causes the loss of the axial signal **S3** and the parallel growth of the rhombic signal **S4** (Figure 2), indicating that primary species **S3** converts into **S4**. The latter disappears after annealing at ~230 K (not shown), and no new mixed-valent EPR signal was detected. A similar annealing pattern is shown by $[DS_{ox}-$**2**-ACP$]_{mv}$. Possible reasons of the instability of the mixed-valence forms of DS will be considered below.

Taken together, these data demonstrate that two equilibrium conformers coexist in solution of DS complexes with **1**-ACP and its thia analogue. Relaxation of the $[DS_{ox}]_{mv}$ structure to a thermally equilibrated mixed-valence structure shifts this equilibrium toward the conformer giving the more anisotropic rhombic EPR signals, **S4** and **S7,** respectively.

^{1}H ENDOR Spectroscopy. We employed 35 GHz ^{1}H ENDOR spectroscopy to characterize the diiron sites of $[DS_{ox}]_{mv}$ and $[DS_{ox}-$**1**-ACP$]_{mv}$ in greater detail. Figure 3 shows ^{1}H ENDOR spectra taken at $g_2 = 1.926$ of the major $[DS_{ox}]_{mv}$ conformer in H_2O and D_2O buffers. Comparison of the spectra shows that proton resonances with hyperfine coupling values $A \leq 5$ MHz belong mostly to nonexchangeable, constitutive protons (*27*). The resonances with larger hyperfine coupling values belong to protons exchangeable in D_2O. Both a terminal H_2O ligand to the Fe(III) ion and a hydroxo-bridge base can give rise to an exchangeable ^{1}H doublet with $A_{max} \approx 16-17$ MHz (*27*, *28*). However, the low *g*-anisotropy of the EPR signal indicates that an oxo, not a hydroxo, bridge is present, and the ^{1}H ENDOR spectrum can be well simulated by assuming that two equivalent protons reside on terminal water bound to Fe(III) (Figure 3 and Figure S4, Supporting Information).

Comparison of the experimental and simulated spectra presented in Figure 3 also suggests the presence of another exchangeable proton the signal of which is strongly overlapped with that of the water ligand coordinated to Fe(III). This signal has a hyperfine coupling $A_{obs} \approx 6-8$ MHz that changes little with field (Figure S4, Supporting Information). A similar signal was observed for the mixed-valent form of MMO and was assigned to terminal water ligated to Fe(II) of the cryoreduced cluster (*27*).

This assignment also is consistent with ^{1}H ENDOR data for cryoreduced *E. coli* RNR protein R2. Diferric R2 is known to have terminal water ligands on both μ-oxo-bridged Fe ions (*29*), and thus one expects that ^{1}H ENDOR spectra of cryoreduced protein R2 should show proton signals from terminal water ligands bound to both iron(III) and iron(II)

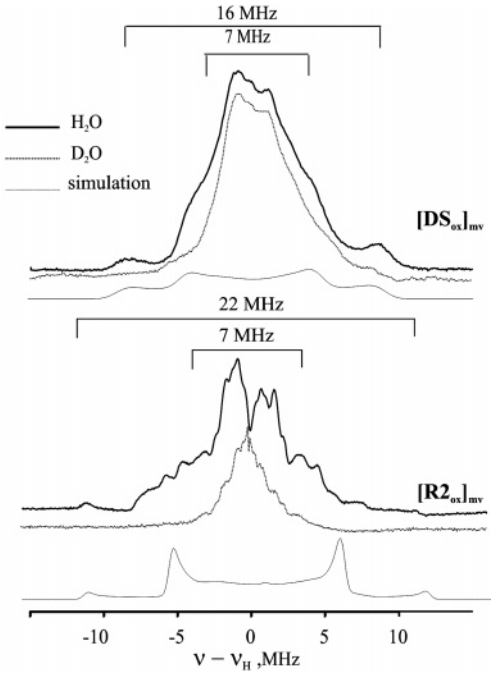

FIGURE 3: CW ^{1}H ENDOR spectra of cryoreduced DS_{ox} and met-RNR protein R2 in H_2O (—) and D_2O buffers (•••) taken at g_2. The simulated spectra are shown by thin lines. Simulation parameters were as follows: for DS, $A = [-9, -9, 18]$ MHz, $\gamma = 60°$, $\beta = 75°$; for R2 protein $A = [11, -11, 22]$, $\gamma = 0°$, $\beta = 40°$ and $\gamma = 70°$, $\beta = 70°$. Instrument conditions were as follows: $T = 2$ K; MW frequency = 35 GHz; modulation amplitude = 1.3 G; MW power = 30 dB; RF power = 10 W; scan speed = 0.5 MHz/s; 60 kHz broadening of rf excitation.

of the mixed-valence cluster. The ^{1}H ENDOR spectrum of $[R2_{ox}]_{mv}$ presented in Figure 3 reveals a strongly coupled exchangeable proton doublet, $A_{max} \approx 20$ MHz, which is assigned to water coordinated to Fe(III). The 2-D field-frequency ^{1}H ENDOR pattern for this water is well simulated under the assumption of the presence of two nonequivalent protons (Figure S5). Figure 3 also shows a more isotropic exchangeable proton signal with $A \approx 6-8$ MHz that is better resolved than those for $[DS_{ox}]_{mv}$ and that is assigned to a water coordinated to the Fe(II). Taken together, these results thus indicate that each iron ion of the DS_{ox} active site coordinates a water ligand, in agreement with current views (*5*−*7*).

The ^{1}H ENDOR spectrum for the dominant primary mixed-valence species **S3** of the $[DS_{ox}-$**1**$-$ACP$]_{mv}$ complex (Figure 4) also shows an exchangeable ^{1}H ENDOR signal from a terminal water coordinated to Fe(III). The hyperfine coupling, $A_{max} \approx 21.5$ MHz (Figure 4, Figure S6A in Supporting Information), is slightly greater than the corresponding value for the water ligand of $[DS_{ox}]_{mv}$; as shown in the Supporting Information (Figure S6B), the ^{1}H ENDOR pattern for this water ligand is simulated by assuming two nonequivalent protons (Figure S6). This simulation further suggests the presence of another exchangeable ^{1}H ENDOR signal, $A \approx 8$ MHz, that may be identified as water coordinated to iron(II) (*27*). The $[DS_{ox}-$**2**-ACP$]_{mv}$ complex shows ^{1}H ENDOR spectra that are very similar to these for cryoreduced DS$-$**1**-ACP complex (Figure 4) and are interpreted similarly.

As discussed above, the minority species **S4** in the $[DS_{ox}-$substrate$]_{mv}$ complex (Table 1) becomes dominant after

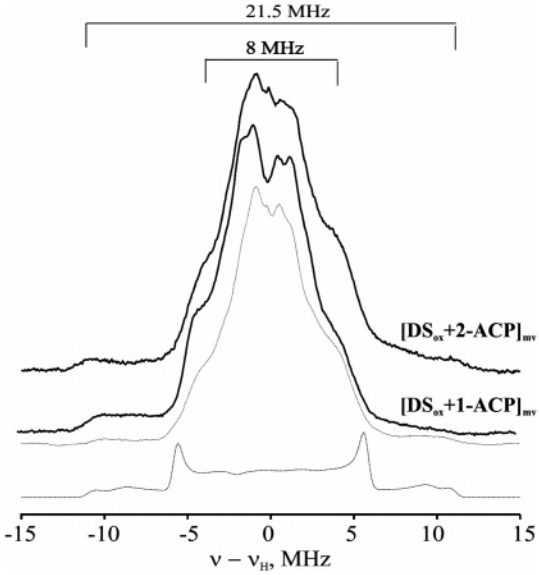

FIGURE 4: CW ^{1}H ENDOR spectra of cryoreduced DS$_{ox}$−**1**-ACP and DS$_{ox}$−**1**-ACP complexes in H_2O (—) and D_2O buffers (•••) taken at $g = 1.924$. (Below) Simulation for one proton with parameters as follows: $A = [-11.5, -11.5, 23]$ MHz; $\gamma = 60°$, $\beta = 65°$ and $\gamma = 60°$, $\beta = 55°$. Instrument conditions were the same as those in Figure 3.

annealing to 170−200 K. The ^{1}H ENDOR spectra for this species, presented in Figure 5, has a maximum breadth of less than 9 MHz, noticeably less than the breadth for the majority species (Figure 4). The diiron cluster that yields this **S4** mixed-valence species thus has neither a terminal water coordinated to Fe(III) nor a μ-OH$^-$ bridge, as either of these would give signals from strongly coupled exchangeable protons with $A_{max} > 16$ MHz. The **S4** ^{1}H ENDOR spectra of Figure 5 reveal nearly an isotropic proton signal with $A \approx 8$ MHz; the sample in D_2O shows a ^{2}H ENDOR signal with $A \approx 1.2$ MHz that matches well, showing that this proton is exchangeable. Such proton(s) may be assigned to terminal water coordinated to Fe(II) on the basis of the *A*-value. Thus, in the relaxed mixed-valent **S4** and **S7** species formed by annealing [DS$_{ox}$−**1**-ACP]$_{mv}$ and [DS$_{ox}$−**2**-ACP]$_{mv}$ complexes, the Fe of the diiron cluster that does *not* accept the electron loses a terminal water ligand and the μ-oxo bridge remains unprotonated.

*^{14}N ENDOR of [DS$_{ox}$]$_{mv}$ and Its Complexes with **1**-ACP and **2**-ACP*. The histidines bound to the diiron center of [DS$_{ox}$]$_{mv}$ have been examined through CW Q-band ^{14}N ENDOR studies (Figure 6); for comparison, CW Q-band ^{14}N ENDOR spectra are presented for the mixed-valent cluster of cryoreduced R2 protein. Each ^{14}N ENDOR spectrum of Figure 6 is assigned as ν_+ transitions of two histidine nitrogen nuclei, one bound to the Fe(III) and one to the Fe(II); as described elsewhere (*27*), in Q-band ENDOR it is not uncommon to observe only the ν_+ branch. The maximum hyperfine coupling and quadrupole splitting for the Fe(II)Fe(III) cluster of the cryoreduced R2 protein are observed at $g_\perp = 1.82$: for the histidine nitrogen coordinated to the ferrous ion, $A_{max} = 3.16$ MHz and $3P_{zz} = 2.4$ MHz; for the histidine coordinated to Fe(III), $A_{max} = 7.31$ MHz and $3P_{zz} = 2.3$ MHz. The ^{14}N ENDOR spectra of cryoreduced RNR R2 are much sharper than those of cryoreduced DS and its complexes; however, the histidine nitrogen coordinated to Fe(II) of cryoreduced DS has $A_{max} = 3.34$ MHz and $3P_{zz} = 2.1$ MHz, and the histidine nitrogen coordinated to Fe(III) has $A_{max} = 9.1$ MHz and $3P_{zz} = 2.9$ MHz, which are close to the values for cryoreduced protein R2.

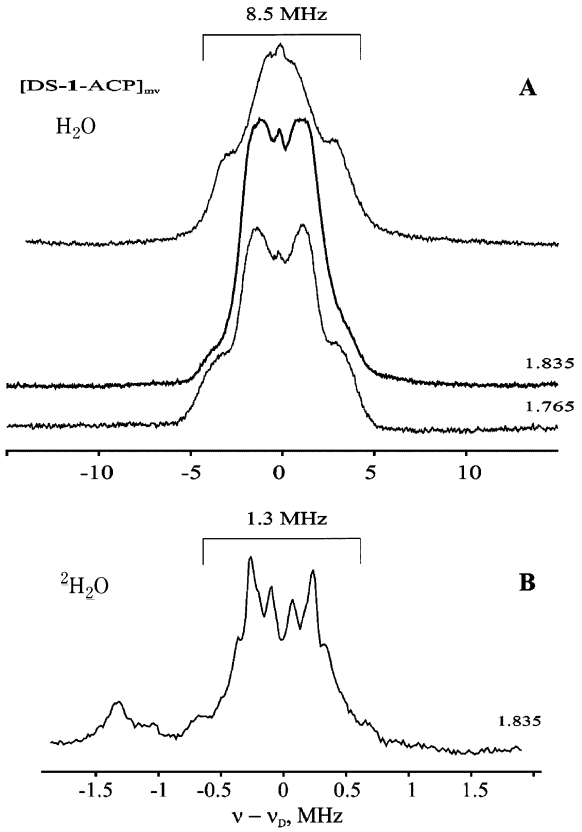

FIGURE 5: Panel A shows CW ^{1}H ENDOR spectra at $g_1 \approx 1.895$, $g_2 = 1.835$, $g_3 = 1.765$ of cryoreduced DS$_{ox}$−**1**-ACP complexes in H_2O annealed at 175 K for 1 min. Instrument conditions were the same as those in Figure 3. Panel B shows ^{2}H 35 GHz MIMS pulse ENDOR of the sample at $g_2 = 1.835$. Instrument conditions were as follows: MIMS sequence with a $\pi/2$ microwave pulse = 50 ns, 60 μs rf pulse, $\tau = 452$ ns, 34.711 GHz, $g = 1.835$; pulse sequence repetition time = 25 ms; 40 averaged data shots per point; 20 scans.

^{14}N ENDOR spectra of the cryoreduced DS−**1**-ACP and DS−**2**-ACP complexes, both primary cryoreduction product and annealed centers, are qualitatively similar to those for [DS$_{ox}$]$_{mv}$ (Figure 6). However, the intensities of these spectra are a factor of 2−3 lower than those for cryoreduced DS. Indeed, all the mixed-valent forms of DS and its complexes studied show much broader and less intense ^{14}N ENDOR spectra than those for the structurally similar diiron cluster in the cryoreduced R2 protein. It is likely that these spectroscopic differences indicate that the geometry of Fe−N(His) bonds in DS are much less sharply defined than those in R2.

DISCUSSION

The EPR and ENDOR data presented here for the cryoreduced DS$_{ox}$ show that the diiron cluster of dominant [DS$_{ox}$]$_{mv}$ conformer contains a μ-oxo bridge and thus the diiron site in the DS$_{ox}$ precursor also has such a bridge, in agreement with other studies (*5*−*8*). The weak broad mixed-valent signal(s) seen in the EPR spectrum of cryoreduced DS arise from cryoreduction of minority DS$_{ox}$ conformers, which have been detected by Mossbauer and EXAFS

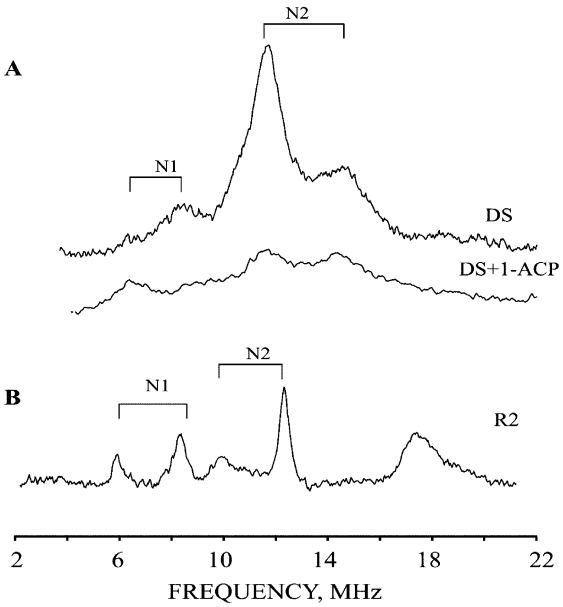

FIGURE 6: Panel A shows CW ^{14}N 35 GHz ENDOR spectra of cryoreduced DS and DS−**1**-ACP (1:2) taken at $g = 1.894$ and 1.924, respectively. Panel B shows ^{14}N 35 GHz ENDOR spectrum of cryoreduced *E. coli* RNR protein R2 taken at $g = 1.82$. Instrument conditions were as follows: $T = 2$ K; modulation amplitude = 1.5 G; RF power = 20 W, scan speed = 0.5 MHz/s; 100 kHz broadening of rf excitation.

spectroscopy in DS_{ox} (∼28−30% of the total DS), which suggested that they contain μ-hydroxo-bridged diferric cluster(s) (*8*); their low EPR intensity makes it impossible to characterize them by EPR. The weakness of the EPR signal(s) from these cryoreduced conformers is in large part caused by their low population and in part by the fact that a μ-hydroxo-bridged diiron cluster is characterized by highly anisotropic **g** tensor(s) with a broad signal and a correspondingly low amplitude; it might also reflect a lower cryoreduction yield.

The ^{1,2}H and ^{14}N ENDOR data show that DS_{ox} is like diferric RNR protein R2 in that each iron of the μ-oxo bridged Fe(III,III) cluster is coordinated by terminal water and histidine ligands, in agreement with existing views (*5*−*7*). In cryoreduced DS, the μ-oxo-bridge gets protonated upon annealing to 170 K, and the EPR signal disappears upon annealing to temperatures above 230 K. Similar annealing behavior was reported for cryoreduced *E. coli* RNR protein R2 (*12*). The R2 protein does not form a stable mixed-valence form at ambient temperatures (*30*), and we have not succeeded in generating an EPR-active mixed-valence form of DS or its **1**-ACP complex with chemical reductants (dithionate and methylviolgen). It seems most likely that in such cases the mixed-valence species disproportionates to form diferric and diferrous states.

The EPR spectra of DS_{ox} cryoreduced in the presence of stoichiometric amounts of **1**-ACP or **2**-ACP are consistent with other studies, which indicate that substrate has high affinity for resting DS_{ox}(*31*), just as seen for binding **1**-ACP to DS_{red} (*10*). Binding **1**-ACP or **2**-ACP significantly alters the **g** tensors of the cryoreduced diiron site. For the binding of noncoordinating substrates/analogues to cause such changes in parameters, they must be inducing conformational changes in the DS_{ox} active site upon binding. Two distinct EPR signals for both $[DS_{ox}-substrate]_{mv}$ complexes reflect the presence in solution of two types of equilibrium DS_{ox}−substrate conformers. The ENDOR data show that the dominant substrate-bound DS conformer(s) (giving rise to the axial EPR signal **S3** or **S5**) still contain a μ-oxo-bridged diferric center in which each iron ion has one histidine and one water in its coordination sphere. However, ENDOR parameters for these terminal ligands are distinct from these in resting $[DS_{ox}]_{mv}$, suggesting that substrate binding affects the coordination geometry of these terminal ligands. The mixed-valence forms, $[DS_{ox}]_{mv}$, contain a high-spin ferric ($S = {}^5/_2$) and high-spin ferrous ($S = 2$) ion produced by the reduction, and these are antiferromagnetically coupled to give a ground spin state of $S = {}^1/_2$. For strong antiferromagnetic coupling, the **g** tensor of the $S = {}^1/_2$ diiron cluster can be described to a good approximation as

$$\mathbf{g} = {}^7/_3\mathbf{g}_{Fe(III)} - {}^4/_3\mathbf{g}_{Fe(II)} \quad (2)$$

where symbols have their usual meaning (*32*). The ferric-ion **g** tensor is largely invariant upon changes to its coordination geometry, while the **g** tensor of the ferrous ion is not. Thus, the changes in the **g** tensor of the spin-coupled center upon substrate/inhibitor binding disclose perturbations at the Fe(II) site but do not rule out effects at Fe(III). On assuming an isotropic g value for Fe(III) $S = 2.03$, the g-values for DS (Table 1) and eq 2 lead to the calculated result, $\mathbf{g}_{Fe(II)} = [2.093, 2.109, 2.129]$. Substrate perturbations of the **g** tensor (Table 1) primarily change g_3 (Table 1) as a consequence of changes in g_3 for the uncoupled Fe(II), as expected (*32*); DS−**1**-ACP has the biggest shift in g_3, caused by a change to $(g_{Fe(II)})_3 = 2.257$. It is interesting that binding of **1**-ACP and **2**-ACP produces slightly different effects on the spectroscopic properties of the cryoreduced diferric site. This means that even a slight modification to the stearoyl group exerts a noticeable effect on the geometry and consequently the electronic structure of the diiron center.

It is interesting to note that the μ-oxo bridge of the $[DS_{ox}-substrate]_{mv}$ complex remains unprotonated during annealing to 230 K. In the majority of cryoreduced μ-oxo-bridged diiron clusters that we have studied, which includes those in various proteins as well as model compounds, including DS_{ox}, the μ-oxo ligand protonates on annealing to temperatures below 190 K (*12*, *13*, *24*). The influence of the bound substrate of DS in inhibiting this protonation suggests that the μ-oxo bridge has become kinetically less accessible to receipt of a proton from the active-site pocket. As in the case of of DS_{mv}, the disappearance of the signal for $[DS-substrate]_{mv}$ above 230 K is likely preceded by protonation of the μ-oxo bridge.

Taken together, these observations show that substrate binding results in protein-mediated changes of the diiron site geometry at the ferric ion that becomes reduced during cryoreduction and possibly at both and that these changes are sensitive to the chemical structure of substrate. Furthermore the data show that the structure of the one-electron reduced active site of DS−substrate complex does not bind water and presumably is five-coordinate suggests that this state probably is closer to that in diferrous state, which has the same characteristics (*10*), that is, binding substrate likely preorganizes the active site in such a way as to favor its reduction and reactivity toward dioxygen.

ACKNOWLEDGMENT

We thank Prof. H. Halpern, Pritzker School of Medicine, University of Chicago, for access to the ^{60}Co irradiator.

SUPPORTING INFORMATION AVAILABLE

Figures of EPR spectra. This material is available free of charge via the Internet at http://pubs.acs.org.

REFERENCES

1. Shanklin, J., and Cahoon, E. B. (1998) Desaturation and related modifications of fatty acids, *Annu. Rev. Plant Physiol. Plant Mol. Biol. 49*, 611−641.
2. Lindquist, Y. V. (2001) in *Handbook of Metalloproteins* (Messerschmidt, A., and Huber, R., Eds.) pp 725−737, John Wiley & Sons, Ltd.
3. Moche, M., Shanklin, J., Ghoshal, A., and Lindqvist, Y. (2003) Azide and Acetate Complexes Plus Two Iron-depleted Crystal Structures of the Di-iron Enzyme Δ^9 Stearoyl-Acyl Carrier Protein Desaturase: Implications for Oxygen Activation and Catalytic Intermediates, *J. Biol. Chem. 278*, 25072−25080.
4. Shanklin, J., and Somerville, C. (1991) Stearoyl-acyl-carrier-protein desaturase from higher plants is structurally unrelated to the animal and fungal homologs, *Proc. Natl. Acad. Sci. U.S.A. 88*, 2510−2514.
5. Fox, B. G., Shanklin, J., Somerville, C., and Munck, E. (1993) Stearoyl-acyl carrier protein Δ^9 desaturase from *Ricinus communis* is a diiron-oxo protein, *Proc. Natl. Acad. Sci. U.S.A. 90*, 2486−2490.
6. Fox, B. G., Shanklin, J., Ai, J., Loehr, T. M., and Sanders-Loehr, J. (1994) Resonance Raman Evidence for an Fe−O−Fe Center in Stearoyl-ACP Desaturase. Primary Sequence Identity with Other Diiron-Oxo Proteins, *Biochemistry 33*, 12776−12786.
7. Lyle, K. S., Moenne-Loccoz, P., Ai, J., Sanders-Loehr, J., Loehr, T. M., and Fox, B. G. (2000) Resonance Raman Studies of the Stoichiometric Catalytic Turnover of a Substrate-Stearoyl-Acyl Carrier Protein Δ^9 Desaturase Complex, *Biochemistry 39*, 10507−10513.
8. Shu, L., Broadwater, J. A., Achim, C., Fox, B. G., Munck, E., and Que, L., Jr. (1998) EXAFS and Mossbauer characterization of the Diiron(III) site in stearyl-acyl carrier protein Δ^9-desaturase, *JBIC, J. Biol. Inorg. Chem. 3*, 392−400.
9. Lindqvist, Y., Huang, W. J., Schneider, G., and Shanklin, J. (1996) Crystal structure of Delta(9) stearoyl-acyl carrier protein desaturase from castor seed and its relationship to other di- iron proteins, *EMBO J. 15*, 4081−4092.
10. Yang, Y.-S., Broadwater, J. A., Pulver, S. C., Fox, B. G., and Solomon, E. I. (1999) Circular Dichroism and Magnetic Circular Dichroism Studies of the Reduced Binuclear Non-Heme Iron Site of Stearoyl-ACP Δ^9-Desaturase: Substrate Binding and Comparison to Ribonucleotide Reductase, *J. Am. Chem. Soc. 121*, 2770−2783.
11. Broadwater, J. A., Ai, J., Loehr, T. M., Sanders-Loehr, J., and Fox, B. G. (1998) Peroxodiferric Intermediate of Stearoyl-Acyl Carrier Protein Δ^9 Desaturase: Oxidase Reactivity during Single Turnover and Implications for the Mechanism of Desaturation, *Biochemistry 37*, 14664−14671.
12. Davydov, R., Kuprin, S., Graslund, A., and Ehrenberg, A. (1994) EPR study of the mixed-valent diiron center in E. coli RNR produced by reduction of radical-free protein R2 at 77 K, *J. Am. Chem. Soc. 116*, 11120−1128.
13. Davydov, R., Sahlin, M., Kuprin, S., Graslund, A., and Ehrenberg, A. (1996) Effect of the tyrosyl radical on the reduction and structure of the E. coli RNR protein R2 diferric site as probed by EPR of the mixed-valent state produced at 77 K, *Biochemistry 35*, 5571−5576.
14. Davydov, R., Davydov, A., Ingemarson, R., Thelander, L., and Ehrenberg, A. (1997) EPR study of the mixed-valent diiron sites in the mouse and Herpes simplex virus RNR produced by radiolityc reduction at 77 K, *Biochemistry 36*, 9093−9100.
15. Davydov, R., Valentine, A. M., Komar-Panicucci, S., Hoffman, B. M., and Lippard, S. J. (1999) An EPR Study of the Dinuclear Iron Site in the Soluble Methane Monooxygenase from *Methylococcus capsulatus* (Bath) Reduced by One Electron at 77 K: The Effects of Component Interactions and the Binding of Small Molecules to the Diiron(III) Center, *Biochemistry 38*, 4188−4197.
16. Shanklin, J. (2000) Overexpression and Purification of the *Escherichia coli* Inner Membrane Enzyme Acyl-Acyl Carrier Protein Synthase in an Active Form, *Protein Expression Purif. 18*, 355−360.
17. Broadwater, J. A., and Fox, B. G. (1999) Spinach Holo-Acyl Carrier Protein: Overproduction and Phosphopantetheinylation in *Escherichia coli* BL21(DE3), in Vitro Acylation, and Enzymic Desaturation of Histidine-Tagged Isoform I, *Protein Expression Purif. 15*, 314−326.
18. Behrouzian, B., Shanklin, J., and Buist, P. H. (2001) Application of KIE and thia approaches in the mechanistic study of a plant stearoyl-ACPΔ9 desaturase, *Chem. Commun.*, 401−402.
19. Bollinger, J. M., Stubbe, J., Huynh, B. H., and Edmondson, D. E. (1991) Novel Diferric Radical Intermediate Responsible for Tyrosyl Radical Formation in Assembly of the Cofactor of Ribonucleotide Reductase, *J. Am. Chem. Soc. 113*, 6289−6291.
20. Davydov, R., Makris, T. M., Kofman, V., Werst, D. W., Sligar, S. G., and Hoffman, B. M. (2001) Hydroxylation of Camphor by Reduced oxy-Cytochrome P450cam: Mechanistic Implications of EPR and ENDOR of Catalytic Intermediates in Native and Mutant Enzymes, *J. Am. Chem. Soc. 123*, 1403−1415.
21. Werst, M. M., Davoust, C. E., and Hoffman, B. M. (1991) Ligand Spin Densities in Blue Copper Proteins by Q-band ^{1}H and ^{14}N ENDOR Spectroscopy, *J. Am. Chem. Soc. 113*, 1533−1538.
22. Abragam, A., and Bleaney, B. (1970) *Electron Paramagnetic Resonance of Transition Metal Ions*, 2nd ed., Clarendon Press, Oxford, U.K.
23. DeRose, V. J., and Hoffman, B. M. (1995) in *Methods in Enzymology* (Sauer, K., Ed.) pp 554−589, Academic Press, New York.
24. Davydov, R. M., Smieja, J., Dikanov, S. A., Zang, Y., Que, L., Jr., and Bowman, M. K. (1999) EPR properties of mixed-valent μ-oxo and μ-hydroxo dinuclear iron complexes produced by radiolytic reduction at 77 K, *JBIC, J. Biol. Inorg. Chem. 4*, 292−301.
25. Davydov, R. M., Menage, S., Fontecave, M., Graslund, A., and Ehrenberg, A. (1997) Mixed-valent μ-oxo-bridged diiron complexes produced by radiolytic reduction at 77 K studied by EPR, *JBIC, J. Biol. Inorg. Chem. 2*, 242−255.
26. Mizoguchi, T. J., Davydov, R. M., and Lippard, S. J. (1999) Structural and Spectroscopic Comparisons between (μ-Oxo)- and (μ-Hydroxo)bis(.mu.-carboxylato)diiron(III) Complexes That Contain All-Oxygen-Donor Ligands, *Inorg. Chem. 38*, 4098−4103.
27. DeRose, V. J., Liu, K. E., Lippard, S. J., and Hoffman, B. M. (1996) Investigation of the Dinuclear Fe Center of Methane Monooxygenase by Advanced Paramagnetic Resonance Techniques: On the Geometry of the DMSO Binding, *J. Am. Chem. Soc. 118*, 121−134.
28. Willems, J.-P., Lee, H.-I., Burdi, D., Doan, P. E., Stubbe, J., and Hoffman, B. M. (1997) Identification of the Protonated Oxygenic Ligands of Ribonucleotide Reductase Intermediate X by Q-band ^{1,2}H CW and Pulsed ENDOR, *J. Am. Chem. Soc. 119*, 9816−9824.
29. Logan, D. T., Su, X. D., Aberg, A., Regnstrom, K., Hajdu, J., Eklund, H., and Nordlund, P. (1996) Crystal structure of reduced protein R2 of ribonucleotide reductase: The structural basis for oxygen activation at a dinuclear iron site, *Structure 4*, 1053−1064.
30. Andersson, K. K., and Graslund, A. (1995) Diiron−Oxygen Proteins, *Adv. Inorg. Chem. 43*, 359−408.
31. Haas, J. A., and Fox, B. G. (2002) Fluorescence Anisotropy Studies of Enzyme−Substrate Complex Formation in Stearoyl-ACP Desaturase, *Biochemistry 41*, 14472−14481.
32. Bertrand, P., Guigliarelli, B., and More, C. (1991) The Mixed-Valence [Fe(III), Fe(II)] Binuclear Centers of Biological Molecules Viewed through EPR Spectroscopy, *New J. Chem. 15*, 445−454.

BI048599T